measurably. This can be attributed to fluctuating predominant flows in the bifurcated submerged entry nozzle with a low tundish filling level. Inclusion distribution is associated with the casting stream. A high-volume stream of steel conveys more inclusions than a low-volume stream. Reoxidation may also occur simultaneously. The inclusions consist essentially of alumina, with small percentages of calcium oxide and titanium oxide.

(A2006139; received on 5 Jul, accepted on 7 Aug 2006)

References

[1] J. Szekely and N.J. Themelis: Rate Phenomena in Process Metallurgy, John Wiley & Sons, New York 1971, pp. 515/56.

[2] F. Kemeny, D.J. Harris, A. McLean, T.R. Meadowcroft and J.D. Young: Fluid Flow Studies in the Tundish of a Slab Caster. In: Continuous Casting of Steel, Proceedings 2nd Process Technology Conference, February 23 to 25, 1981, Chicago, Vol. 2 (1981) [Ed.:] ISS-AIME, pp. 232/245.

[3] L.J. Heaslip and A. McLean: "Tundish Metallurgy" - Considerations Pertaining to Tundish Performance and Metallurgical Treatment During Continuous Casting. In: 39th Electric Furnace Conference Proceedings, Houston, Dec. 8-11, 1981, Vol. 39, ISS-AIME, pp. 333/337.

[4] Y. Sahai and R. Ahuja: Ironmaking and Steelmaking, 13 (1986) No. 5, 241/247.

[5] A. Diener, E. Görl, W. Pluschkell and K.D. Sardemann: Steel Research, 61 (1990), No. 10, 449/454.

[6] M.T. Burns, J. Schade, W.A. Brown and K.R. Minor: I & SM, 1992, Nov., 35/39.

[7] B. Hoh, H. Jacobi, H.-E. Wiemer, K. Wünnenberg: Stahl u. Eisen, 109 (1989), No. 2, 41/48.

[8] R. Jauch, H. Jacobi, H. Litterscheidt, W. Pluschkell, P. Valentin, K. Wünnenberg: Stahl u. Eisen, 109 (1989), No. 6, 269/276.

[9] H. Jacobi, H.-J. Ehrenberg, K. Wünnenberg: Stahl u. Eisen, 118 (1998), No. 11, 87/95.

[10] O. Levenspiel: "Chemical Reaction Engineering", 2nd edition, John Wiley & Sons, Inc., New York, 1962.

[11] H. Jacobi, K. Wünnenberg: ECSC Project 7210-CC112/113 (P 3504, Concluding Report).

[12] K. Wünnenberg: Stahl u. Eisen, 120 (2000), No. 7, 29/35.

Investigation of Orientation Gradients in Pearlite in Hypoeutectoid Steel by use of Orientation Imaging Microscopy

Tetsuya Takahashi, Dirk Ponge, Dierk Raabe

Max-Planck-Institut für Eisenforschung, Düsseldorf, Germany

The microstructure of pearlite in hypoeutectoid steel was investigated using high resolution orientation imaging microscopy. Systematic orientation gradients were observed along the longitudinal direction within the pearlitic ferrite lamellae. Corresponding orientation gradients seemed to occur also in the cementite within the same pearlite colony. The orientation gradients in the ferrite strongly correlated with the local topographical curvature of the pearlitic colony. The orientation relationship between the ferrite and the cementite lamellae was constant even in areas with strong orientation gradients.

Keywords: Pearlite, orientation gradient, texture, steel, EBSD, orientation imaging microscopy.

Introduction

For steels and related ferrous alloys containing pearlite, the precise microstructural characterization of pearlite is of great importance since it significantly contributes to the mechanical properties of the material. The yield strength of pearlite depends on its interlamellar spacing. Refining that spacing entails an increase in strength which follows a Hall-Petch type relation [1,2]. Beyond the contribution of the interlamellar spacing, the strength of pearlite was reported to depend as well on the prior austenite grain size and on the pearlite colony size although these effects were considered to be small [3]. In contrast to these findings Ray and Mondal [4] observed that the strength of pearlite in *hypoeutectoid* steels does not follow a Hall-Petch type relation. They reported that the strength of pearlite in the hypoeutectoid steels varied considerably even when the interlamellar spacings in the pearlite colonies are almost constant. They attributed that variation in the strength of the pearlite in the hypoeutectoid steels to the influence of hydrostatic stresses exerted by the presence of proeutectoid ferrite in the material.

Besides the morphological parameters such as interlamellar spacing, prior austenite grain size, and pearlite colony size, other microstructural factors such as the amount of elements in solid solution and the dislocation density in the ferrite have been commonly taken into account when evaluating the strength of pearlite. The influence of the substructure and of the crystallographic texture of the pearlite, however, have not been sufficiently considered in that context yet. The contributions of these influencing factors were up to now only evaluated on the basis of regression analysis by which possible scattering of the strength of the pearlite constituents due to the presence of microstructural heterogeneities was simply averaged over the whole pearlite volume rather than studied in detail.

It is a common observation though that the lamellar structure in a pearlite colony is not always homogeneous, but rather contains various types of substructures even in the as-transformed state. Puttick [5] has identified several kinds of growth faults in the lamellae of the pearlite colonies. These include linear discontinuities in the cementite lamellae; branched crystallization; deviations of lamellar orientation; rod-like growth; and growth of round cementite inclusions. Bramfitt and Marder [6] have also studied the substructural faults of pearlite colonies. They showed that areas with higher dislocation densities and extended dislocation substructures in the pearlitic ferrite were sometimes associated

with a discontinuity in the growth of that pearlite colony. They also found other substructural features. These included dislocations at the cementite/ferrite interface; discontinuities in those cementite lamellae containing a high density of dislocations; and growth steps inside the cementite lamellae. Structural faults were also observed within the pearlitic cementite. For instance, Koreeda and Shimizu [7] observed dislocations and low angle tilt boundaries which consisted of uniformly spaced dislocations in the cementite phase of annealed pearlite.

When reviewing these various observations on the micro- and nanostructure of pearlite one may conclude that the influence of the inner structure of the pearlite lamellae on the strength of the material has been underestimated so far. Rather it seems likely that the variation of the substructure in each pearlite colony may be responsible for the variations of the strength which have been reported in some of the investigations quoted above. For example, it is well conceivable that a pearlite colony containing a large number of dislocations, cells, or subgrains may show higher strength than a colony with a small defect density. A more detailed study of the substructure is, hence, pertinent to improve our understanding of the strength of pearlite.

The quantitative, systematic, and representative characterization of substructures in a pearlite colony is a challenge. For instance, although conventional transmission electron microscopy (TEM) is obviously well suited for a detailed analysis of individual structural defects such as dislocation substructures in pearlitic ferrite, the volume that can be probed by it is obviously limited. As an alternative, microstructure investigation via orientation imaging microscopy which is based on the electron back scattered diffraction (EBSD) technique [8] provides a good possibility to overcome that limitation. Measuring EBSD maps in a high resolution scanning electron microscope allows for the quantitative characterization of the microstructure of large areas. Relevant characteristics obtained from such scans include the topography, microtexture, and local misorientations in a pearlite colony. Despite of these obvious advantages only few EBSD studies have been conducted so far on pearlite [9].

The purpose of the present study is to conduct a high resolution EBSD analysis of the inner structure of pearlite with the aim to show the presence of characteristic crystallographic orientation pattern in the pearlite colonies and to discuss the importance of this aspect on the mechanical properties of hypoeutectoid and related eutectoid steels.

Experimental

The material used in this investigation is a commercial hypoeutectoid steel, Fe-0.42C-0.7Mn-0.2Si (wt%). A cylindrical sample with a diameter of 4 mm and a length of 9 mm was machined. The sample was austenitized at 1223 K for 10 minutes and subsequently cooled down at a cooling rate of 0.09 K/s using He gas. The cross section of the sample was mechanically polished to #4000 emery paper and then electrically polished using a perchloric acid solution to remove surface defects introduced by the mechanical polishing. The use of diamond paste for fine mechanical polishing was avoided in order to prevent fracture and deformation of the characteristic fine lamellar structure of the pearlite.

The samples were studied using a combination of scanning electron imaging microscopy and orientation microscopy via electron diffraction for a precise and complete characterization of the material at a scale ranging from several mm down to the nm regime. Particularly by the high resolution automatic mapping of crystal orientations and phases it is possible to study such crystalline microstructures and textures in a detail that cannot be reached by any other technique.

The instrument that was used for these measurements, particularly with regard to the orientation microscopy, was the high resolution, high-intensity field emission scanning electron microscope (FEGSEM) SEM JEOL JSM 6500 F. With this instrument extremely high beam currents at high spatial resolution can be reached due to a special construction of the field emission gun (FEG). This system was used for the high-speed and high-precision measurement of electron backscatter diffraction (EBSD) patterns and EDX spectra. The instrument was equipped with a highly sensitive, high speed digital CCD camera (DigiView) for EBSD pattern recording and software programmes for automatic crystal orientation mapping (ACOM - OIM 3 software by TSL) and phase analysis (Delphi software by TSL). The system allows obtaining a lateral resolution of the orientation determination of about 25 to 200 nm depending on the material inspected. Up to 60 orientation measurements per second can be obtained depending on sample preparation.

The actual measurements performed in this study on pearlite were conducted at an accelerating voltage of 15kV and an emission current of around 100nA. Crystallographic orientation mappings of the ferrite phase were taken using a step size of 200 nm. The quality of the EBSD pattern from pearlitic cementite was insufficient so that a detailed nanotexture mapping was only conducted in the ferritic lamellae of the pearlite. The continuous maps of the nanotexture in the ferrite lamellae were reconstructed by systematically mapping for each point probed (200 nm step size) the Miller indices for one of main the crystallographic axis as outlined in the ensuing section. The high density of the diffraction spots and corresponding crystal orientation data provides a crystallographic high resolution map which allows for a detailed analysis of orientation patterning and orientation gradients. Further details of the used high resolution EBSD setup and the techniques used for generating the texture maps can be found in references [10-18].

Results

Figure 1a shows a SEM micrograph of a representative portion of the pearlitic microstructure. After electrical polishing, the microstructural constituents are clearly visible without any subsequent treatment. The microstructure consists of globular proeutectoid ferrite formed mostly at prior austenite grain boundaries and lamellar pearlite composed of alternating plates of ferrite (pearlitic ferrite) and cementite (pearlitic cementite). This is a typical microstructure of hypoeutectoid steel when subjected to slow cooling from the austenite state.

Focusing on the pearlitic region in the micrograph, one can notice not only an ideal lamellar structure, i.e. continuous straight and parallel lamellae, but also several microstructural inhomogeneities such as lamellar discontinuities and shape changes of the lamellae. The areas with such discontinuous topography changes coincide with regions revealing a more pronounced substructure inside the lamellae. **Figure 1b** shows an orientation map which was obtained from the corresponding area of the SEM micrograph. The colour code shows the crystallographic normal vector in conjunction with the inverse pole figure. The interface characterization is also illustrated in the orientation map. The grain boundaries are classified into large angle boundaries with a misorientation higher than 15° and low angle boundaries with a misorientation between 2° to 15°. One should note that the orientation map does not contain the analysis of the pearlitic cementite but reveals only the texture of the ferrite.

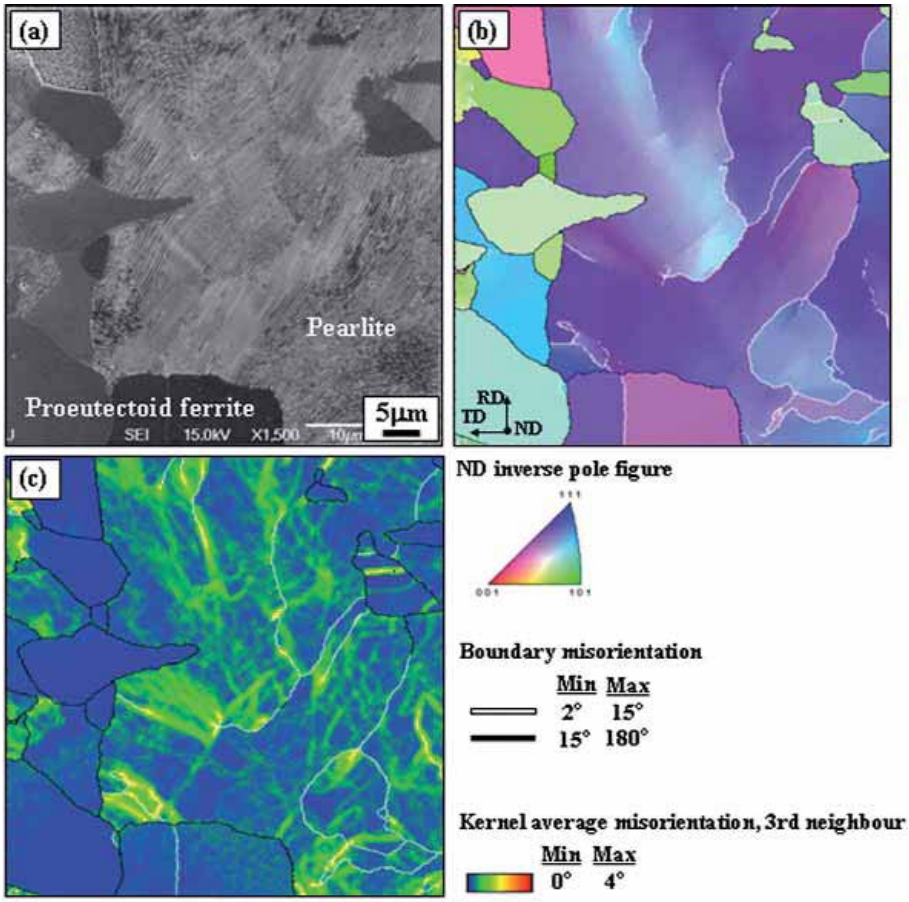

Figure 1. Microstructure of the hypoeutectoid steel. (a) SEM micrograph. (b) Microtexture mapping in terms of the inverse pole figure (IPF) colour code of the crystallographic normal vector. (c) Kernel average misorientation map using orientations up to the 3rd neighbour shell.

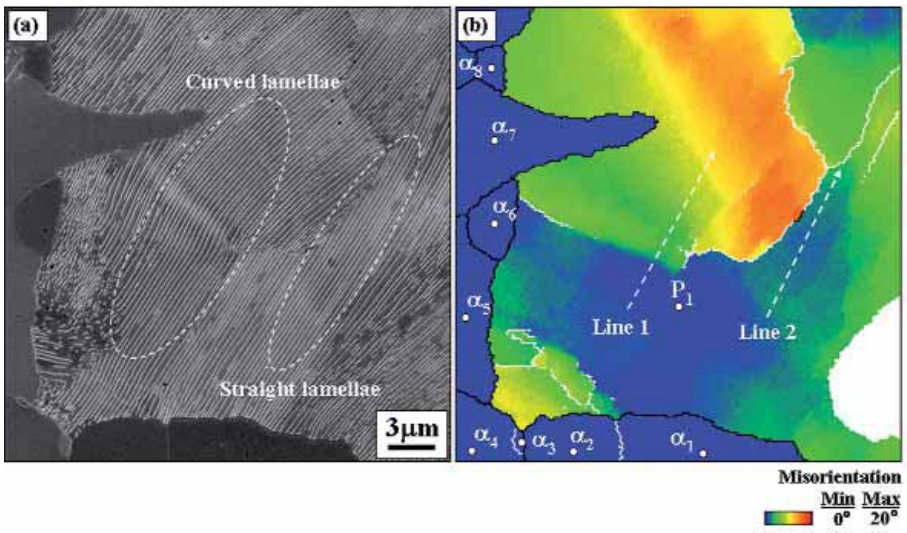

Figure 2. Magnified image of the lower left part of Figure 1. (a) SEM micrograph. (b) Corresponding grain internal misorientation map indicating orientation gradients of up to 15° in the same colony.

The proeutectoid ferrite grains are separated mostly by large angle grain boundaries and reveal an almost random crystallographic texture. Only some of the grains are separated by low angle boundaries. No substructure boundaries were found inside the proeutectoid ferrite grains.

In contrast to the proeutectoid ferrite grains, the ferrite inside the pearlite colonies contains subboundaries as also expected from the SEM micrograph. These subboundaries are usually characterized as low angle boundaries. The subboundaries are not always continuous to completely separate the individual pearlite colonies, but sometimes resolved into structures with misorientations below 2° which was used as a lower cut-off angle in this analysis. This observation means that new pearlite colonies do not necessarily have to be formed by a nucleation process as individual colonies, but they may also be created by changing the lamellar direction during the growth process.

Another significant feature is the existence of long range continuous crystallographic orientation changes within the pearlitic regions without the presence of sharp subboundaries. This means that a certain amount of dislocations must exist inside the pearlite colonies since the continuous large

changes in the orientations as observed in this work can only be created by the accumulation of corresponding polarized dislocation arrangements which are referred to as geometrically necessary dislocations (GNDs) [19-21].

Figure 1c illustrates the Kernel average misorientation map of the same area. The map is constructed by calculating the average misorientation of every measurement point up to its third nearest neighbour EBSD point. The Kernel average misorientation map reveals short range orientation gradients. This type of measure allows one to relate localized orientation changes and certain spatial misorientation pattern to dislocation substructures such as cells or subboundaries. Figure 1c clearly reveals that the pearlitic regions are characterized by a much higher density of zones with strong local orientation gradients than the proeutectoid ferrite grains. The distribution of the magnitude of the Kernel average misorientation is not uniform throughout the pearlitic region, but shows pronounced patterning. The sort of network structure of the distribution can also be observed.

For a more quantitative analysis of the spatial distribution of changes in the crystallographic orientation in the pearlitic ferrite, **Figures 2a and 2b** provide a magnified image of the lower left part of Figure 1 together with the corresponding grain internal misorientation map, respectively. The colours represent the misorientation measured from each reference point inside the colony. Regions which are completely separated by grain boundaries having a misorientation of at least 2° were regarded as individual crystals in this analysis. The grain internal misorientation was determined for eight individual proeutectoid ferrite grains and one pearlite colony, where the orientation reference points are denoted by α_1 to α_8 for the proeutectoid ferrite and P_1 for the pearlitic ferrite, respectively. Figure 2b clearly shows that inside the pearlitic region pronounced long range orientation gradients exist. In contrast no misorientation gradients were observed inside the proeutectoid ferrite grains surrounding the pearlite colony.

The changes in the crystallographic orientations are not of a stochastic character, but they are quite systematic. One can observe continuous changes in the crystallographic orientation of up to 15° within the same pearlite colony. Also, the orientation changes have a specific direction, i.e. they form homogeneous orientation gradients. It seems from the corresponding SEM micrograph that the lateral pattern of the orientation changes is related to the morphology of the lamellae in the pearlite colony.

Figure 3 reveals the misorientation profile along two different lines which are shown in Figure 2b. A misorientation profile is expressed as the change in the crystallographic orientation relative to the orientation of the starting point which serves as a reference. Line 1 is placed in lamellae with a strong crystallographic curvature and Line 2 in a region with a much weaker crystallographic curvature. The data reveal that the development of the misorientation profiles is consistent with the corresponding morphological characteristics of the lamellae.

The inspected misorientation profile along the curved lamellae (Line 1) can be described by a continuous change in the crystallographic orientation with roughly three separate regions, namely, one with very small, one with large, and one with medium orientation changes. The variation in the magnitude of the orientation gradients agrees well to the variation of the curvature of the lamellar morphology: Along Line 1, the morphology of the lamella is straight followed by an S-shaped portion. At the end of the probed area it reveals a modest crystallographic curvature.

In the mid part of the profile the orientation change is very steep showing about 4° orientation change over a distance of 2 μm. Although this area appears from the colour map in Figure 2 at first view as a zone with a rather abrupt orientation change it is not identical to a small angle grain boundary owing to the fact that the orientation gradient is not localized but continuous, i.e. the change in orientation is smeared out over about 2 μm.

This misorientation profile also suggests that there is a correlation between the morphological lamellar curvature and the change in crystallographic orientation of the pearlitic ferrite. The misorientation profile along line 2 shows a small crystallographic orientation change relating to the straight morphological shape of the lamella.

Up to this point, it is uncertain whether the pearlitic cementite also exhibits the same course of the orientation changes as the pearlitic ferrite since the orientation map in the present study does not include any systematic crystallographic information from the cementite lamellae. **Figure 4** gives an example of an EBSD analysis of the crystallographic orientations for both the pearlitic ferrite and cementite along a strongly curved portion of pearlite. The spot analysis was performed at two different positions for both phases. The positions of the measurement are denoted by α_1, α_2 for the pearlitic ferrite and θ_1, θ_2 for the pearlitic cementite. The crystallographic orientations at these positions are shown in a {100} pole figure to identify the orientation relationship between the two phases in the pearlite. It should be mentioned though that, even by spot EBSD

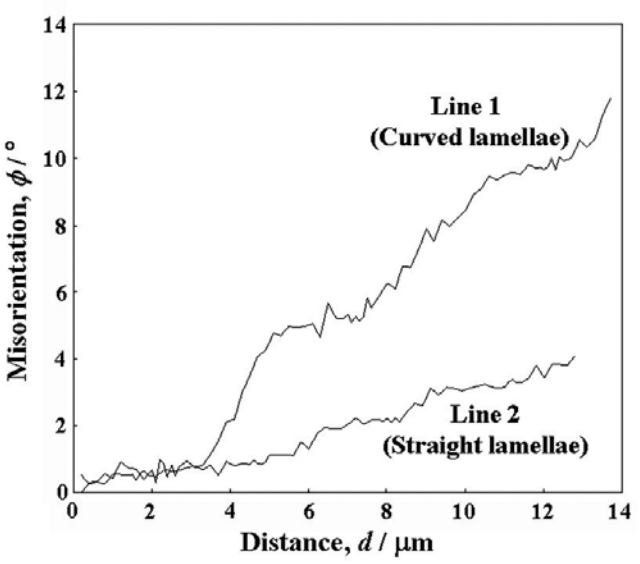

Figure 3. Misorientation profile along Line 1 and Line 2 illustrated in Figure 2.

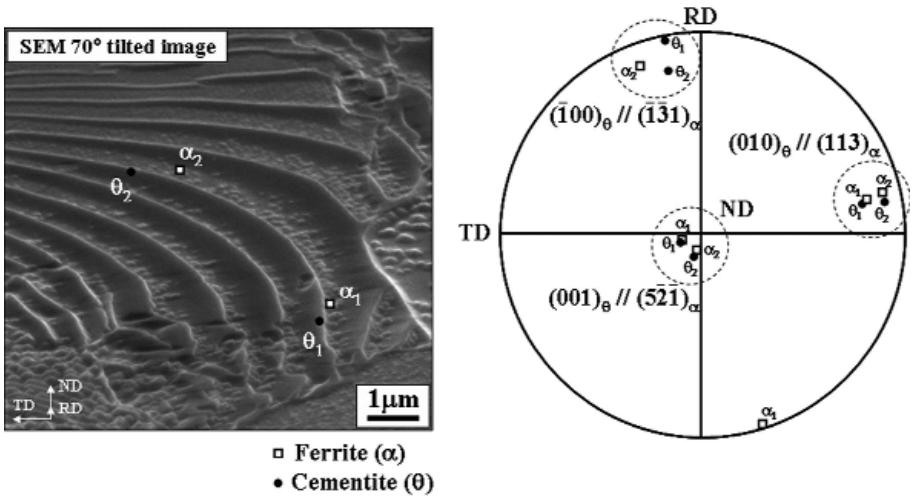

Figure 4. EBSD analysis of ferrite and cementite in a pearlite region with considerable topographical lamellar curvature. (a) 70° tilted (around TD) SEM image showing the positions of the EBSD measurements. (b) Orientations determined for every measurement point represented in the form of a {100} pole figure.

analysis, it was not always possible to obtain a good EBSD pattern quality from the cementite as required for the determination of the orientation with sufficient accuracy. The quality of the EBSD pattern from the cementite seems to be dependent on the size of the lamellae, the lamellar orientation with respect to the sample surface as well as the etching condition.

It is important to note that at positions 1 and 2 which are located along the curvature of a single lamella we observed different crystallographic orientations both, of the pearlitic ferrite and of the pearlitic cementite. In spite of the substantial change in the crystallographic orientations of both phases along the curved lamella from position 1 to position 2, the ferrite/cementite orientation relationship remains almost unchanged. The misorientation between positions 1 and 2 amounts to approximately 10° which is obviously beyond the range of possible measurement errors of the EBSD method.

It is known that the ferrite/cementite orientation relationship in pearlite is mostly that of either the Isaichev relationship [22], the Pitsch-Petch relationship [23,24], or the Bagaryatsky relationship [25]. In the present investigation, the experimentally observed ferrite/cementite orientation relationship is closest to the one suggested by Pitsch and Petch [23,24]. This orientation relationship is described by

$$[100]_\theta \ 2.6^\circ \text{ from } [13\bar{1}]_\alpha$$
$$[010]_\theta \ 2.6^\circ \text{ from } [113]_\alpha$$
$$[001]_\theta // \quad [5\bar{2}\bar{1}]_\alpha$$

where the subscript α stands for the ferrite and θ for the cementite. Although the relationship we observe is close to these values, it deviates by somewhat more than 5° for the $[100]_\theta$ vector. We observe the same result for the orientation relationship in different interface regions, i.e. the orientation relationship between ferrite and cementite in the pearlite tends to be the same even when large orientation gradients exist inside a colony.

Discussion

Formation of crystallographic orientation gradients in pearlite colonies. As already indicated in the previous section the observation of orientation gradients in the pearlitic ferrite and very likely also in the cementite implies that the pearlite colonies contain a large density of geometrically necessary dislocations (GNDs). This conclusion is also covered by the Kernel average misorientation map which reveals pronounced local discontinuous orientation changes that must be matched by corresponding accumulations of GNDs. Furthermore, the present results show that the magnitude of the orientation gradients is closely related to the variation in the morphological lamellar curvature.

Usually GNDs are generated due to deformation gradients induced by externally imposed constraints associated with plastic deformation. In the current case, however, no external forces were exerted. Also internal forces, for instance such as created during cooling owing to differences in the thermal expansion coefficients, are not likely to have such an enormous effect entailing the orientation gradients observed, since the neighbouring ferrite grains do not reveal any orientation changes in their interiors. If the pearlite would have been plastically deformed severely due to an internal constraint during heat treatment, the neighbouring proeutectoid ferrite grains, whose yield strength is much lower than that of pearlite, should have been deformed as well to a certain extent. Similarly, in such a case, compatibility consideration would suggest the co-deformation of the proeutectoid ferrite grains and of the pearlite. Therefore, it is suggested that the GNDs as well as the lamellar curvature are formed in the course of the growth of pearlite during the phase transformation.

Bramfitt and Marder [6] have discussed the possibility of dislocation sources that may be responsible for the formation of substructural faults in the pearlite. Those include the possibility of inheritance of dislocations from the parent austenite phase; the stresses created by the dynamics of the phase transformation itself; the effect of the different crystal structures; and the effect of cooling from the transformation temperature. However, it is still uncertain which of those mechanisms may be most relevant for the generation of the GNDs and the lamellar curvature in the pearlite colonies since they may act simultaneously.

Although the origin of the GNDs is still uncertain, it is quite obvious that the morphological lamellar curvature can be realized by the joint crystallographic rotation of both the pearlitic ferrite and cementite through the incorporation of the GNDs as schematically illustrated in **Figure 5a**.

In contrast to the present result, it has been observed in the electron microscope that striations, also characterized as

growth steps, occur at ferrite/cementite interface when the cementite lamellae change their growth direction [6,26]. Detailed TEM studies by Hackney and Shiflet [27,28] have also demonstrated that the ferrite/cementite interface contains steps, also referred to as direction steps, ~ 5 nm high in areas with strong lamellar curvature. Based on their observations, it was believed that those steps were responsible for the formation of curved lamellar shapes without any necessity for a crystallographic rotation inside the ferrite matrix as observed in this work. In this concept the preferred crystallographic orientation relationship between the ferrite and the cementite in the pearlite could also be maintained everywhere at the interface. The schematic illustration of the step or ledge mechanism for the formation of the lamellar curvature is shown in **Figure 5b** for comparison with the mechanism that we suggest.

It should be emphasised that in both suggested mechanisms (Figure 5), the ferrite/cementite interface remains unchanged during the development of any lamellar curvature. This strong tendency to preserve the crystallography of the ferrite/cementite interface can be probably attributed to the strong anisotropy of its interfacial energy [26,28]. This means that a strong tendency should exist for the growing lamellae to maintain the preferred ferrite/cementite orientation relationship (Isaichev, Pitsch-Petch, or Bagaryatsky) to minimize the total interface energy.

It seems that both mechanisms, the GNDs mechanism suggested in this study and the step mechanism suggested before, may in principle explain the observed curvatures of the lamellar shapes. Using TEM technique, however, it is practically impossible to carry out a long range systematic analysis of the crystallographic orientation changes of the ferrite or cementite along the lamellar curvature. Since we observed such pronounced orientation gradients, it is clear that the step or ledge mechanism alone cannot be responsible for the phenomena observed, since it does not include any such crystallographic gradient.

It is, therefore, conceivable that the two different mechanisms may play a role at two different scales. It is plausible that the step mechanism is responsible for the short range accommodation of the lamellar curvature at a microscopic scale while the GND mechanism contributes to the formation of the long range curvature by means of crystallographic accommodation at a mesoscopic scale.

Influence of orientation gradients on the strength of pearlite colonies. Although the real mechanism for the generation of GNDs during the pearlite growth is still unknown, the present results imply that the strength of the pearlite constituent depends not only on the morphological parameters such as interlamellar spacing, prior austenite grain size, and pearlite colony size, but also on the amount of GNDs in every pearlite colony.

When assuming a strongly curved pearlite colony such as observed in Figure 2a, one can approximate the density of GNDs according to the simple geometrical model of a beam under pure bending [19-21],

$$\rho = \frac{\kappa}{b} \tag{1}$$

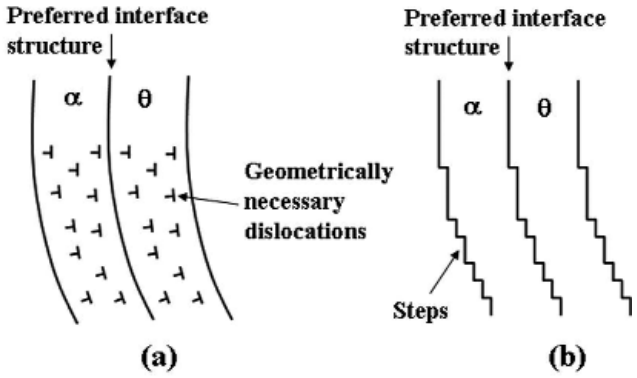

Figure 5. Two different possible mechanisms to accommodate the lamellar curvature. (a) Crystallographic rotation mechanism. (b) Interface step mechanism.

where κ is the plastic curvature imposed by the bending and b is the magnitude of the Burgers vector. The plastic curvature κ can be approximated using the rotation angle of the crystal ϕ and the lateral length of the beam L, i.e.

$$\rho = \frac{\phi}{bL} \tag{2}$$

The results of Figure 3 showed that the crystallographic orientation change of the pearlitic ferrite amounts to about 10° over a distance of 12.5 μm. Using Eq. (2), the density of the GNDs in this curved lamella can be estimated as 6×10^{13} m^{-2} where a value of 0.248 nm was used for the Burgers vector of iron. The contribution of the dislocation density ρ on the strength σ can be calculated as

$$\sigma = \alpha G b \sqrt{\rho} \tag{3}$$

where α is a constant, G the shear modulus and b the magnitude of the Burgers vector. Using values of 0.38 [29], 81×10^3 MPa, and 0.248 nm for α, G and b, respectively, a value of 59 MPa is obtained for σ. In the light of the strength range of pearlite from 300 to 900 MPa depending mainly on the interlamellar spacing, the contribution of 59 MPa on the strength seems to be so high that the influence of the orientation gradient should not be neglected.

In the light of this result, one may conclude the large scatter observed in the strength of pearlite may depend on the amount of GNDs in the structure. More specific, it is highly likely that a pearlite colony containing a larger fraction of curved lamellae will yield a higher strength than that containing less curved lamellae because of the difference in the density of GNDs it contains. This applies even if the other conventional morphological parameters of pearlite are identical. It is also expected that a high density of GNDs will increase the rate of cementite spheroidization during ferrite soft annealing treatments.

Conclusions

In the present study orientation imaging microscopy via EBSD has been employed to study the substructural features of pearlite constituents in hypoeutectoid steel. The results have revealed the existence of orientation gradients of

the pearlitic ferrite and presumably also in the cementite. These results suggest that a certain density of geometrically necessary dislocations is present in the pearlite colonies matching the curvatures observed. The lateral distribution of the orientation gradients in the ferrite, i.e. also of the geometrically necessary dislocations, was found to be quite heterogeneous. In addition, a strong correlation between the crystallographic orientation gradients and the morphological lamellar curvatures was established.

It is suggested that the microstructural parameters widely used for pearlite characterization including interlamellar spacing, austenite grain size, and pearlite colony size are not sufficient to fully describe the structure and the mechanical strength of pearlite. For a better understanding of the mechanical properties of pearlite, the heterogeneous distribution of the geometrically necessary dislocations in every pearlite colony should also be considered or at least an average value for their density.

(A2006054; received on 17 Feb 2006, accepted on 27 March 2006)

Contact: Prof. Dr.-Ing. habil. D. Raabe
Max-Planck-Institut für Eisenforschung
Max-Planck-Str. 1
40237 Düsseldorf / Germany
Email: raabe@mpie.de

References

[1] T. Gladman, I. D. Mcivor and F. B. Pickering: J. Iron Steel. Inst., 210 (1972), 916.
[2] T. Takahashi and M. Nagumo: Trans. Jpn. Inst. Met., 11 (1970), 113.
[3] J. M. Hyzak and I. M. Bernstein: Metall. Trans. A, 7A (1976), 1217.
[4] K. K. Ray and D. Mondal: Acta Metall. Mater., 39 (1991), 2201.
[5] K. E. Puttick: J. Iron Steel. Inst., 185 (1957), 161.
[6] B. L. Bramfitt and A. R. Marder: Metallography, 6 (1973), 483.
[7] A. Koreeda and K. Shimizu: Philos. Mag., 17 (1968), 1083.
[8] B. L. Adams, S. I. Wright and K. Kunze: Metall. Trans. A, 24A (1993), 819.
[9] A. W. Wilson and G. Spanos: Materials Characterization, 46 (2001), 407.
[10] R. Song, D. Ponge, D. Raabe and R. Kaspar: Acta Mater., 53 (2005), 845.
[11] S. Zaefferer: Mater. Sci. Forum, 495-497 (2005), 3.
[12] D. Raabe, M. Sachtleber, Z. Zhao, F. Roters, S. Zaefferer: Acta Mater., 49 (2001), 3433.
[13] D. Raabe, M. Sachtleber, H. Weiland, G. Scheele, Z. Zhao: Acta Mater., 51 (2003), 1539.
[14] N. Chen, S. Zaefferer, L. Lahn, K. Günther, D. Raabe: Acta Mater., 51 (2003), 1755.
[15] S. Zaefferer, J.-C. Kuo, Z. Zhao, M. Winning, D. Raabe: Acta Mater., 51 (2003), 4719.
[16] I. Thomas, S. Zaefferer, F. Friedel, D. Raabe: Advanced Engin. Mater., 5 (2003), 566.
[17] J. Konrad, S. Zaefferer, D. Raabe: Acta Mater., 54 (2006), 1369.
[18] N. Zaafarani D. Raabe, R. N. Singh, F. Roters, S. Zaefferer: Acta Mater., 54 (2006), 1707.
[19] J. F. Nye: Acta Metall., 1 (1953), 153.
[20] A. Ma F. Roters D. Raabe: Acta Mater., in press, 2006.
[21] A. Ma F. Roters D. Raabe: Acta Mater., in press, 2006.
[22] I. V. Isaichev: Zh. Tekh. Fiz., 17 (1947), 835.
[23] W. Pitsch: Acta Metall., 10 (1962), 79.
[24] N. J. Petch: Acta Cryst., 6 (1953), 96.
[25] Y. A. Bagaryatsky: Dokl. Akad. Nauk. SSSR., 73 (1950), 1161.
[26] F. C. Frank and K. E. Puttick: Acta Metall., 4 (1956), 206.
[27] S. A. Hackney and G. J. Shiflet: Acta Metall., 35 (1987), 1019.
[28] S. A. Hackney and G. J. Shiflet: Scripta. Metall., 20 (1986), 389.
[29] T. N. Baker: in Yield, Flow and Fracture of Polycrystals (edited by T. N. Baker), Applied Science, London 1983, 235.